Phys. Lett. B 872 (2026) 140099

Contents lists available at ScienceDirect

Physics Letters B

journal homepage: www.elsevier.com/locate/physletb

Letter

Search for a dark baryon in the $\Xi^- \to \pi^- +$ invisible decay

BESIII Collaboration [1]

ARTICLE INFO

Editor: Maurizio Pierini

Keywords:
BESIII
Dark baryon
Invisible decay

ABSTRACT

A search for a dark baryon is performed for the first time in the two-body decay $\Xi^- \to \pi^- +$ invisible using $(10.087 \pm 0.044) \times 10^9$ J/ψ events collected at a center-of-mass energy of $\sqrt{s} = 3.097$ GeV with the BESIII detector at the BEPCII collider. No significant signal is observed, and the 90% (95%) confidence level upper limits on the branching fraction $\mathcal{B}(\Xi^- \to \pi^- +$ invisible) are determined to be 4.2×10^{-5} (5.2×10^{-5}), 6.9×10^{-5} (8.4×10^{-5}), 6.5×10^{-4} (7.6×10^{-4}), 1.1×10^{-4} (1.3×10^{-4}) and 4.5×10^{-5} (5.5×10^{-5}), under the dark baryon mass hypotheses of 1.07 GeV/c^2, 1.10 GeV/c^2, m_Λ (1.116 GeV/c^2), 1.13 GeV/c^2, and 1.16 GeV/c^2, respectively. The constraints obtained on the Wilson coefficients $C^L_{us,s}$ and $C^R_{us,s}$ are more stringent than the previous limits derived from the LHC searches for the colored mediators.

1. Introduction

The existence of dark matter (DM) is strongly supported by astrophysical and cosmological observations, yet its nature remains one of the unsolved problems within the Standard Model (SM) of particle physics. One hint to its identity is the similarity between the DM and baryon densities, $\rho_{\rm DM} \approx 5.4\,\rho_{\rm baryon}$ [1], suggesting a potential connection between their origins and motivating the existence of dark sector particles charged under a baryon gauge symmetry with masses at the GeV/c^2 scale [2,3]. The baryonic dark sector has been further motivated by a long-standing discrepancy between the neutron lifetime measured in beam and bottle experiments, which could be resolved if the neutron decays into dark states carrying baryon number with a branching fraction (BF) at the level of 1% [4]. Furthermore, provided that B mesons decay into dark sector antibaryons with a BF larger than 0.01% [5], the B-Mesogenesis mechanism [6,7] can explain the asymmetry between visible matter and antimatter and also the origin and nature of dark matter.

The dark sector anti-baryon has been searched for in decays of B mesons by the *BABAR* experiment [8,9]. Complementary to this, hyperons offer the opportunity to search for the baryonic dark sector through decays into final states containing dark baryons [10], which appear as missing energy in a detector. Invisible decays of the Λ baryon have been searched for by the BESIII experiment [11], constraining the BF of the $\Lambda \to$ invisible decay to be less than 7.4×10^{-5} at the 90% confidence level (C.L.). Exploring pionic hyperon decays with invisible signatures offers access to a broader range of dark baryon masses and an improved experimental sensitivity [12]. The BF of the pionic decay of the Ξ^- baryon with an invisible signature may be as large as 10^{-3} and is not constrained by the SN 1987A cooling bound [12], thus rendering it a priority target for laboratory searches.

This Letter reports a search for a dark baryon in the two-body decay $\Xi^- \to \pi^- +$ invisible, where the Ξ^- candidate is identified by tagging a $\bar{\Xi}^+$ decaying to $\pi^+\bar{\Lambda}(\to \bar{p}\pi^+)$ on its recoiling side [13]. The analysis exploits around 10^7 $\Xi^-\bar{\Xi}^+$ hyperon pairs produced from $(10.087 \pm 0.044) \times 10^9$ J/ψ decays [14] collected at a center-of-mass (CM) energy of $\sqrt{s} =$ 3.097 GeV with the BESIII detector at the BEPCII collider. The charge-conjugated decay $\bar{\Xi}^+ \to \pi^+ +$ invisible is not investigated in this analysis due to the dominant background from $\bar{\Xi}^+ \to \pi^+\bar{\Lambda}(\to \bar{n}\pi^0)$, where the interactions of antineutrons with the detector material produce widespread showers, complicating accurate simulations and the determination of a clean control sample for corrections. A semi-blind procedure is performed to avoid possible bias, where approximately 10% of the data sample is used to validate the analysis procedures before performing the final analysis on the full data set.

2. BESIII detector and Monte Carlo simulation

The BESIII detector [15] records symmetric e^+e^- collisions provided by the BEPCII storage ring [16] in the CM energy range from 1.84 to 4.95 GeV. The BESIII detector has collected large data samples in this energy region [17]. The cylindrical core of the BESIII detector covers 93% of the full solid angle and consists of a helium-based multilayer drift chamber (MDC), a plastic scintillator time-of-flight system (TOF), and a CsI(Tl) electromagnetic calorimeter (EMC), which are all enclosed in a superconducting solenoidal magnet providing a 1.0 T magnetic field. The magnetic field was 0.9 T in 2012, which affects 11% of the total J/ψ data. The solenoid is supported by an octagonal flux-return yoke with

Contact: besiii-publications@ihep.ac.cn.
[1] Author are listed at the end of this paper.

https://doi.org/10.1016/j.physletb.2025.140099
Received 29 May 2025; Received in revised form 15 October 2025; Accepted 4 December 2025
Available online 19 December 2025

resistive plate counter muon identification modules interleaved with steel. The charged-particle momentum resolution at 1 GeV/c is 0.5%, and the dE/dx resolution is 6% for electrons from Bhabha scattering. The EMC measures photon energies with a resolution of 2.5% (5%) at 1 GeV in the barrel (end-cap) region. The time resolution in the TOF barrel region is 68 ps, while that in the end-cap region is 110 ps. The end-cap TOF system was upgraded in 2015 using multigap resistive plate chamber technology, providing a time resolution of 60 ps, which benefits 87% of the data used in this analysis [18–20].

Simulation samples produced with a GEANT4-based [21] Monte Carlo (MC) package, which includes the geometric description [22–25] of the BESIII detector and the detector response, are used to determine detection efficiencies and to estimate backgrounds. The simulation models the beam-energy spread and initial-state radiation in the e^+e^- annihilations with the generator KKMC [26]. The inclusive MC sample includes the production of the J/ψ resonance incorporated in KKMC. All particle decays are modeled with EVTGEN [27] using BFs either taken from the Particle Data Group [28], when available, or otherwise estimated with LUNDCHARM [29,30]. Final-state radiation from charged final-state particles is incorporated using the PHOTOS package [31]. To study the tagging efficiency of the $\bar{\Xi}^+ \to \pi^+\bar{\Lambda}(\to \bar{p}\pi^+)$ decay, the MC sample of $J/\psi \to \Xi^-(\to \text{anything})\bar{\Xi}^+(\to \pi^+\bar{\Lambda}(\to \bar{p}\pi^+))$ is generated according to its helicity decay amplitudes as detailed in Refs. [32–34]. The signal decay $J/\psi \to \Xi^-(\to \pi^-\chi)\bar{\Xi}^+(\to \pi^+\bar{\Lambda}(\to \bar{p}\pi^+))$ is generated according to its helicity decay amplitudes, where χ designates a dark baryon with an invisible signature and the decay-asymmetry parameter of $\Xi^- \to \pi^-\chi$ is assumed to be the same as that of the $\Xi^- \to \pi^-\Lambda$ decay [33]. To satisfy the kinematic constraints while accounting for the background conditions, the signal events are generated under dark baryon mass (m_χ) hypotheses of 1.07 GeV/c^2, 1.10 GeV/c^2, m_Λ, 1.13 GeV/c^2, and 1.16 GeV/c^2, where the m_Λ is the known mass of the Λ [28].

3. Data analysis

3.1. Analysis method

For the signal decay $\Xi^- \to \pi^- + \text{invisible}$, the Ξ^- hyperon is inferred by reconstructing the $\bar{\Xi}^+$ decay in the events of $J/\psi \to \Xi^-\bar{\Xi}^+$ at $\sqrt{s} = 3.097$ GeV. The $\bar{\Xi}^+$ candidates, which constitute the single-tag (ST) sample, are reconstructed with the dominant decay $\bar{\Xi}^+ \to \pi^+\bar{\Lambda}(\to \bar{p}\pi^+)$. Then the double-tag (DT) event is formed by reconstructing the signal decay $\Xi^- \to \pi^- + \text{invisible}$ in the system recoiling against the reconstructed $\bar{\Xi}^+$ hyperon. The absolute BF of the signal decay is determined by

$$\mathcal{B}(\Xi^- \to \pi^- + \text{invisible}) = \frac{N_{\rm DT}^{\rm obs}/\epsilon_{\rm DT}}{N_{\rm ST}^{\rm obs}/\epsilon_{\rm ST}}, \quad (1)$$

where $N_{\rm ST}^{\rm obs}$ ($N_{\rm DT}^{\rm obs}$) is the observed ST (DT) yield and $\epsilon_{\rm ST}$ ($\epsilon_{\rm DT}$) is the corresponding detection efficiency.

3.2. ST selection and yields

Charged tracks detected in the MDC are required to be within a polar angle (θ) range of $|\cos\theta| < 0.93$, where θ is defined with respect to the z-axis, which is the symmetry axis of the MDC. Particle identification (PID) for charged tracks combines measurements of the specific ionization energy loss (dE/dx) in the MDC and the flight time in the TOF to form likelihoods $\mathcal{L}(h)$ ($h = p, K, \pi$) for each hadron h hypothesis. Tracks are identified as protons (pions) when the proton (pion) hypothesis has the greatest likelihood among these three hypotheses.

To reconstruct $\bar{\Lambda}$ and $\bar{\Xi}^+$ candidates, vertex fits [35] are applied to the $\bar{p}\pi^+$ and the $\bar{\Lambda}\pi^+$ combinations, respectively, given that $\bar{\Lambda}$ and $\bar{\Xi}^+$ have relatively long lifetimes. A vertex fit is performed to obtain the decay vertex of the $\bar{\Lambda}$ ($\bar{\Xi}^+$). The production vertices of the $\bar{\Lambda}$ and $\bar{\Xi}^+$ are the decay vertex of the $\bar{\Xi}^+$ and the e^+e^-interaction point, respectively. A subsequent vertex fit is performed using the parameters of the production vertex, decay vertex, and the $\bar{\Lambda}$ ($\bar{\Xi}^+$) flight direction. To suppress background from non-$\bar{\Lambda}$ (non-$\bar{\Xi}^+$) processes, the decay length of the $\bar{\Lambda}$ ($\bar{\Xi}^+$) is required to be larger than zero. The decay length is the distance from the production vertex to the decay vertex, and negative decay lengths can be caused by the detector resolution. The $\bar{p}\pi^+$ and $\bar{\Lambda}\pi^+$ combinations are chosen with the minimum value of the sum of $|M_{\bar{p}\pi^+} - M_{\bar{\Lambda}}|$ and $|M_{\bar{\Lambda}\pi^+} - M_{\bar{\Xi}^+}|$, and $|M_{\bar{p}\pi^+} - M_{\bar{\Lambda}}|$ is required to be less than 4 MeV/c^2, where $M_{\bar{\Lambda}}$ ($M_{\bar{\Xi}^+}$) is the known mass of the $\bar{\Lambda}$ ($\bar{\Xi}^+$) [28]. The recoiling mass against the reconstructed $\bar{\Xi}^+$ candidate is defined as

$$M_{\bar{\Lambda}\pi^+}^{\rm recoil} = \sqrt{\left(E_{\rm CM} - E_{\bar{\Lambda}\pi^+}\right)^2/c^4 - \vec{P}_{\bar{\Lambda}\pi^+}^2/c^2}, \quad (2)$$

where $E_{\rm CM}$ is the CM energy, and $E_{\bar{\Lambda}\pi^+}$ and $\vec{P}_{\bar{\Lambda}\pi^+}$ are the energy and momentum of the selected $\bar{\Lambda}\pi^+$ system defined in the CM system, which have been corrected during the vertex fits. To further suppress backgrounds, the $M_{\bar{\Lambda}\pi^+}^{\rm recoil}$ is required to be in the Ξ^- signal region, defined as (1.290, 1.345) GeV/c^2, corresponding to the region of approximately three times the resolution around the signal peak.

A binned maximum likelihood fit is performed to the $M_{\bar{\Lambda}\pi^+}$ distribution to obtain the ST yield. In the fit, the signal shape is modeled by the MC-simulated shape convolved with a Gaussian function to account for the resolution difference between data and MC simulation. The signal region is defined as $|M_{\bar{\Lambda}\pi^+} - M_{\bar{\Xi}^+}| < 8$ MeV/c^2. By analyzing the inclusive MC sample with the help of a generic event type analysis tool, TopoAna [36], the peaking background is mainly from $J/\psi \to \gamma\bar{\Xi}^+\Xi^-$ and is estimated to contribute 1199 ± 35 events in the signal region. Other nonpeaking background is described by a second-order Chebyshev polynomial function. The fit result is shown in Fig. 1 and the ST yield extracted from the fit is $(1813.4 \pm 1.4) \times 10^3$ after subtracting the contribution from the $J/\psi \to \gamma\bar{\Xi}^+\Xi^-$ background. The ST detection efficiency is evaluated using the signal MC sample and determined to be $(26.03 \pm 0.03)\%$, where the uncertainty is statistical only. The BF of $J/\psi \to \Xi^-\bar{\Xi}^+$ is calculated according to the observed ST yield and the corresponding ST efficiency and is found to be compatible with the previous BESIII measurement [37] within uncertainties.

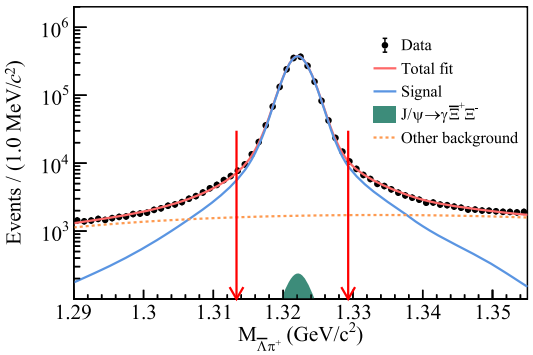

Fig. 1. The $M_{\bar{\Lambda}\pi^+}$ distribution of ST candidates. The black dots with error bars are data and the red solid curve is the fit result. The $J/\psi \to \gamma\bar{\Xi}^+\Xi^-$ peaking background, signal and other nonpeaking background are represented by the green shaded region, blue solid and orange dashed curves, respectively. The red arrows indicate the ST signal window.

3.3. DT selection and yields

The signal decay $\Xi^- \to \pi^- + \text{invisible}$ is searched for using the remaining tracks recoiling against the ST $\bar{\Xi}^+$ candidates. The following criteria are applied to select the signal candidates and suppress the backgrounds mainly from the $\Xi^- \to \pi^-\Lambda(\to p\pi^-)$ and $\Xi^- \to \pi^-\Lambda(\to n\pi^0)$ processes. Exactly one additional negatively charged particle has to be reconstructed for the DT candidate events and it must be identified as a pion. A one-constraint (1C) kinematic fit is performed under the hypothesis of $J/\psi \to \bar{p}\pi^+\pi^+\pi^- + \text{invisible}$. The fit constrains the mass of the

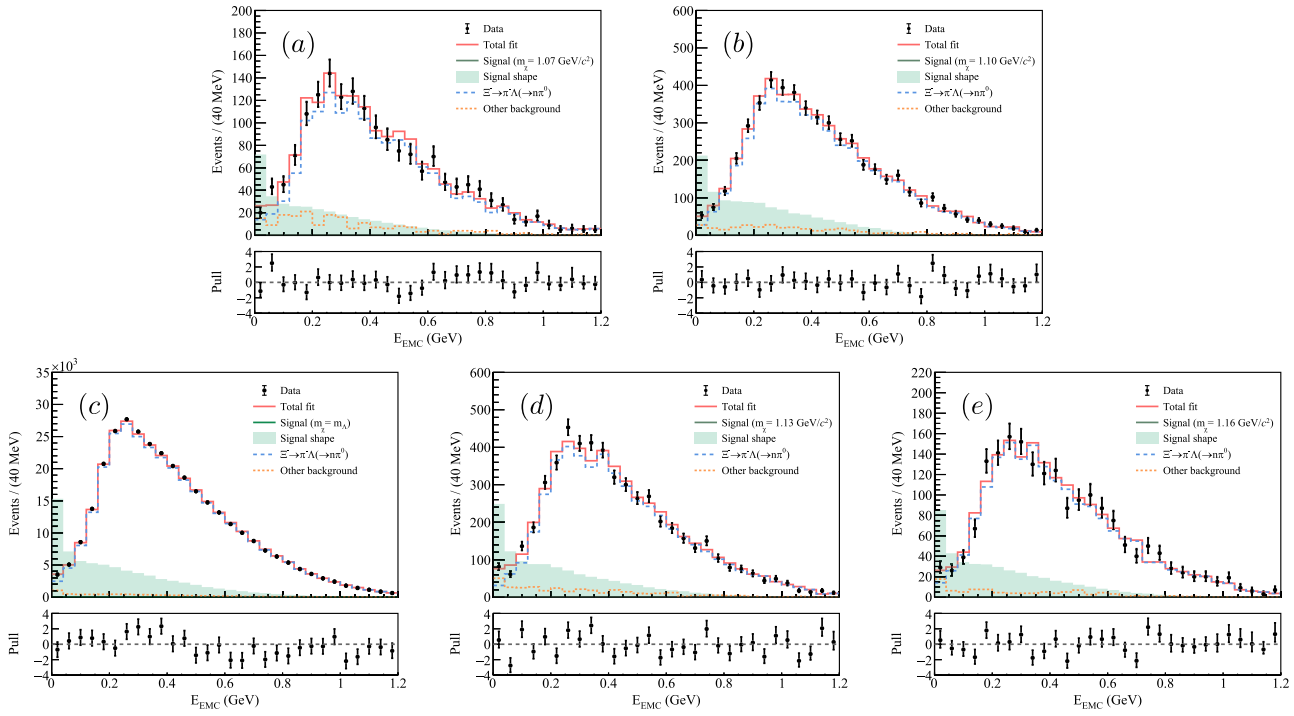

Fig. 2. The fit results of the $E_{\rm EMC}$ distributions under the dark baryon mass hypotheses of (a) $m_{\chi} = 1.07\,{\rm GeV}/c^2$, (b) $m_{\chi} = 1.10\,{\rm GeV}/c^2$, (c) $m_{\chi} = m_{\Lambda}$, (d) $m_{\chi} = 1.13\,{\rm GeV}/c^2$, and (e) $m_{\chi} = 1.16\,{\rm GeV}/c^2$. The black dots with error bars are data points and the red solid lines show the fit results. The signal, signal shape, $\Xi^- \to \pi^-\Lambda(\to n\pi^0)$ background, and other background in the inclusive MC sample are represented by the green solid line, green shaded region, blue dashed line, and orange dashed line, respectively. The signal shape is normalized to BFs of (a) 5×10^{-4}, (b) 2×10^{-3}, (c) 1×10^{-1}, (d) 3×10^{-3}, and (e) 8×10^{-4}. The bottom panels show the fit residuals.

invisible particle to m_{χ}. The χ^2 value of the kinematic fit ($\chi^2_{\pi^-\chi}$) must be less than 20. Except for the case of $m_{\chi} = m_{\Lambda}$, another 1C kinematic fit is performed by constraining the mass of the missing particle to the known Λ mass. The obtained χ^2 value ($\chi^2_{\pi^-\Lambda}$) is required to be larger than $\chi^2_{\pi^-\chi}$. The four-momentum of the DT pion and Ξ^- is obtained from the 1C kinematic fit that constrains the mass of the invisible particle to m_{χ}. The momentum of π^- in the CM frame of Ξ^- (P_{π^-}) is required to lie within lower and upper bounds optimized by maximizing the Punzi significance [38], which is defined as $\varepsilon/(1.5+\sqrt{N_{\rm bkg}})$. Here, ε denotes the signal efficiency obtained from the signal MC sample and $N_{\rm bkg}$ is the number of background events obtained from the background MC samples. The signal momentum windows are determined to be (0.184, 0.192), (0.152, 0.160), (0.132, 0.146), (0.118, 0.126), and (0.070, 0.082) GeV/c under the m_{χ} hypotheses of $1.07\,{\rm GeV}/c^2$, $1.10\,{\rm GeV}/c^2$, m_{Λ}, $1.13\,{\rm GeV}/c^2$, and $1.16\,{\rm GeV}/c^2$, respectively. The DT detection efficiencies are evaluated using the signal MC samples and determined to be $(12.87\pm0.03)\%$, $(11.14\pm0.03)\%$, $(13.25\pm0.04)\%$, $(7.50\pm0.03)\%$ and $(10.28\pm0.03)\%$ under the m_{χ} hypotheses of $1.07\,{\rm GeV}/c^2$, $1.10\,{\rm GeV}/c^2$, m_{Λ}, $1.13\,{\rm GeV}/c^2$, and $1.16\,{\rm GeV}/c^2$, respectively, where the uncertainties are statistical only.

After applying the discussed selection criteria, the dominant background events are from the $\Xi^- \to \pi^-\Lambda(\to n\pi^0)$ process, where the neutron and photon showers from π^0 decays would deposit energy in the EMC. Since the dark baryon has an invisible signature in the detector, the energy sum of all the showers in the EMC, $E_{\rm EMC}$, can be utilized as a discriminator to extract the DT yield. The showers are required to be located in either the barrel region ($|\cos\theta| < 0.80$) or end-cap region ($0.86 < |\cos\theta| < 0.92$). The isolation angle criterion is applied to exclude showers that originate from charged tracks, where the angle subtended by the shower in the EMC and the closest charged track at the EMC must be greater than 10 degrees (20 degrees for $\bar{p}$ tracks since anti-protons interact strongly with nuclei) as measured from the interaction point. To suppress electronic noise and showers unrelated to the event, the difference between the EMC time and the event start time is required to be within [0, 700] ns.

For the signal events, the energy deposit mainly comes from the interaction between the $\bar{p}$ and the detector, under the condition that the induced showers are already suppressed through the isolation angle criteria. However, due to difficulties in accurately modeling anti-proton interactions with the detector material using the GEANT4 package, the raw simulation of $E_{\rm EMC}$ deviates from data [39]. To correct this discrepancy, a control sample of $J/\psi \to \Xi^-(\to \pi^-\Lambda(\to p\pi^-))\bar{\Xi}^+(\to \pi^+\bar{\Lambda}(\to \bar{p}\pi^+))$ is selected and a data-driven approach is applied. The four-momenta of the final state particles in the control sample are obtained through a 6C kinematic fit, where the invariant mass of the $\bar{p}\pi^+$ ($p\pi^-$) combination is constrained to the $\bar{\Lambda}$ (Λ) mass, and the total four-momentum of the final-state particles is constrained to that of the e^+e^- system. The $E_{\rm EMC}$ of signal events is randomly sampled from the shape template obtained from the data control sample, according to the MC-truth information of the momentum and polar angle of the anti-proton. The contribution from additional $p\pi^-$ tracks in the control sample is already estimated and eliminated in the $E_{\rm EMC}$ shape template using an MC sample of $J/\psi \to \Xi^-(\to \pi^-\Lambda(\to p\pi^-))\bar{\Xi}^+(\to \pi^+\bar{\Lambda}(\to \bar{p}\pi^+))$, where only the p and π^- tracks from Λ are allowed to interact with the detector material in the exclusive simulation.

For the background events from $\Xi^- \to \pi^-\Lambda(\to n\pi^0)$, $E_{\rm EMC}$ is divided into two parts, $E^{\pi^0}_{\rm EMC}$ and $E^{\rm other}_{\rm EMC}$. The $E^{\pi^0}_{\rm EMC}$ is the energy from π^0 of the signal side and is obtained through the MC simulation, which describes the interactions of photons or electrons with the material with sufficient accuracy. The $E^{\rm other}_{\rm EMC}$ originates from other sources from charged tracks, neutrons, and noise unrelated to the event. The shape of $E^{\rm other}_{\rm EMC}$ is corrected using a data-driven approach based on a control sample of $J/\psi \to \Xi^-(\to \pi^-\Lambda(\to n\pi^0))\bar{\Xi}^+(\to \pi^+\bar{\Lambda}(\to \bar{p}\pi^+))$. The four-momenta of the final state particles in the control sample are obtained through a 4C kinematic fit, where the neutron is considered as a missing track, the

invariant mass of $\bar{p}\pi^+$ ($n\gamma\gamma$) combination is constrained to the Λ mass, the invariant mass of $\gamma\gamma$ combination is constrained to the π^0 mass, and the total four-momentum of the final-state particles is constrained to that of the e^+e^- system. $E_{\rm EMC}^{\rm other}$ is assigned with a random value from the shape template obtained from the data control sample, according to the MC-truth information of the momentum and polar angle of the anti-proton and neutron. For other background events in the inclusive MC sample, $E_{\rm EMC}$ is corrected using the control sample where Λ decays to either $p\pi^-$ or $n\pi^0$, depending on whether a neutron is involved in the final state.

The corrected distribution of $E_{\rm EMC}$ is used as input in a binned maximum-likelihood fit to determine the DT signal yield. In the fit, the signal, background of $\Xi^- \to \pi^-\Lambda(\to n\pi^0)$, and other backgrounds in the inclusive MC sample are described by their MC-simulated shapes after the data-driven correction. The yields of signal and $\Xi^- \to \pi^-\Lambda(\to n\pi^0)$ background are free to float while the yield of other backgrounds in the inclusive MC sample is fixed. The fit results of $E_{\rm EMC}$ are shown in Fig. 2. No significant signal is observed. The DT yields of $\Xi^- \to \pi^-$ + invisible are determined to be (-13.3 ± 23.9), (-26.9 ± 35.6), (163.5 ± 266.8), (-26.9 ± 37.5), and (-28.3 ± 22.7) under the m_χ hypotheses of 1.07 GeV/c^2, 1.10 GeV/c^2, m_Λ, 1.13 GeV/c^2, and 1.16 GeV/c^2, respectively, where the uncertainties are only statistical.

4. Systematic uncertainty

By employing the DT technique in the analysis, the systematic uncertainties associated with the ST selection can be canceled out. The remaining systematic uncertainties are divided into two types: additive and multiplicative. The additive uncertainties are related to the specific fit methods of DT, while the multiplicative uncertainties are associated with the knowledge of the signal efficiency and ST yields.

When performing the binned maximum-likelihood fit to the $E_{\rm EMC}$ distribution, the uncertainty arising from the choice of bin width is considered by using alternative bin widths of 50 MeV and 30 MeV. The uncertainty due to the signal shape is assigned by considering alternative signal models in which the decay-asymmetry parameter of the $\Xi^- \to \pi^-$ + invisible decay is varied between -1 and 1. The uncertainty due to the background shape of the $\Xi^- \to \pi^-\Lambda(\to n\pi^0)$ process is studied with the alternative background model by changing the decay parameter of the $\Lambda \to n\pi^0$ process by $\pm1\sigma$ [34]. The decay parameter of the $\Lambda \to p\pi^-$ process affects the $\bar{p}$ momentum distribution at the ST side and is varied by $\pm1\sigma$ [33] to obtain the alternative signal and $\Xi^- \to \pi^-\Lambda(\to n\pi^0)$ background shapes. For other backgrounds in the inclusive MC sample, the fixed yield is shifted within $\pm1\sigma$ of statistical uncertainty, and the alternative shape is obtained by smoothing the original shape with the kernel density estimation method [40]. The fit is performed twelve times in total with different methods, and the maximum upper limits (UL) are recorded.

The multiplicative systematic uncertainties are listed in Table 1. The uncertainty due to the ST yield is evaluated by replacing the background shape from a 2nd-order Chebyshev polynomial to a 3rd-order and a 1st-order Chebyshev polynomial function. The uncertainties arising from pion tracking and PID, $\chi^2_{\pi^-\chi}$, $\chi^2_{\pi^-\Lambda} > \chi^2_{\pi^-\chi}$, and P_{π^-} requirements are assigned from studies of a control sample of $\Xi^- \to \pi^-\Lambda(\to n\pi^0)$ decays, where the efficiency difference between data and MC simulation is taken as the uncertainty. The uncertainty of the signal model is obtained from signal MC samples with different decay parameters. By assuming all the sources to be independent, the total multiplicative systematic uncertainties are determined to be 5.1%, 8.3%, 2.9%, 5.3%, and 4.6% under the m_χ hypotheses of 1.07 GeV/c^2, 1.10 GeV/c^2, m_Λ, 1.13 GeV/c^2, and 1.16 GeV/c^2, respectively.

5. Result

Since no significant signal is observed in the data samples, a one-sided frequentist profile-likelihood method [41] is used to compute the expected and observed ULs on $\mathcal{B}(\Xi^- \to \pi^-$ + invisible), where the total multiplicative systematic uncertainty is included in the overall likelihood as a Gaussian nuisance parameter with a width equal to the uncertainty. The 90% (95%) C.L. ULs are determined to be 4.2×10^{-5} (5.2×10^{-5}), 6.9×10^{-5} (8.4×10^{-5}), 6.5×10^{-4} (7.6×10^{-4}), 1.1×10^{-4} (1.3×10^{-4}), and 4.5×10^{-5} (5.5×10^{-5}), under the m_χ hypotheses of 1.07 GeV/c^2, 1.10 GeV/c^2, m_Λ, 1.13 GeV/c^2, and 1.16 GeV/c^2, respectively. The 95% C.L. expected and observed ULs are shown in Fig. 3. The right-handed and left-handed effective operators $\mathcal{O}^R_{us,s}$ and $\mathcal{O}^L_{us,s}$ mediate the decay of Ξ^- into π^- and the dark baryon χ [12], with the corresponding Wilson coefficients denoted as $C^L_{us,s}$ and $C^R_{us,s}$, respectively. The BF of $\Xi^- \to \pi^-\chi$ decay is proportional to the square of the Wilson coefficients. The 95% C.L. ULs on the Wilson coefficients, derived from the results under various m_χ hypotheses, are shown in Fig. 4. The result under the $m_\chi = 1.07$ GeV/c^2 hypothesis corresponds to the 95% C.L. constraints of $C^L_{us,s} < 5.5 \times 10^{-2}$ TeV^{-2} and $C^R_{us,s} < 4.9 \times 10^{-2}$ TeV^{-2}. The constraints obtained on the Wilson coefficients $C^L_{us,s}$ and $C^R_{us,s}$ signif-

Table 1
Summary of multiplicative systematic uncertainties for different m_χ hypotheses.

Source	Uncertainty (%)				
m_χ	1.07 GeV/c^2	1.10 GeV/c^2	m_Λ	1.13 GeV/c^2	1.16 GeV/c^2
ST yield	0.2	0.2	0.2	0.2	0.2
Tracking and PID	1.4	1.4	1.4	1.4	1.4
$\chi^2_{\pi^-\chi}$ requirement	0.1	0.1	0.1	0.1	0.1
$\chi^2_{\pi^-\Lambda} > \chi^2_{\pi^-\chi}$	0.1	5.0	-	4.0	0.1
P_{π^-} requirement	4.7	6.3	1.3	0.2	3.3
Signal model	1.3	1.3	2.2	3.2	2.9
Total (multiplicative)	5.1	8.3	2.9	5.3	4.6

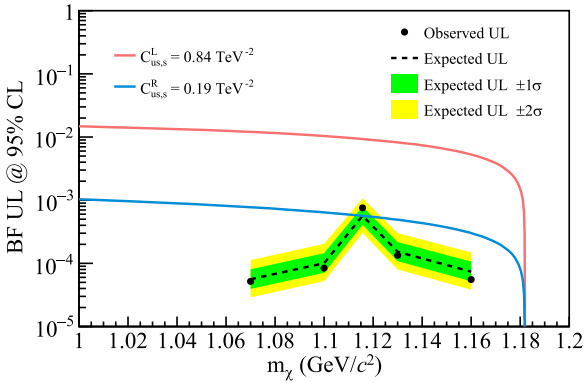

Fig. 3. The expected and observed ULs at the 95% C.L. on the BF of $\Xi^- \to \pi^-$ + invisible under different m_χ hypotheses. The blue and red lines represent the maximum allowed BFs, where the Wilson coefficients are set to $C^L_{us,s} < 0.84\,\text{TeV}^{-2}$ and $C^R_{us,s} < 0.19\,\text{TeV}^{-2}$ derived from the LHC searches for the colored mediators [12].

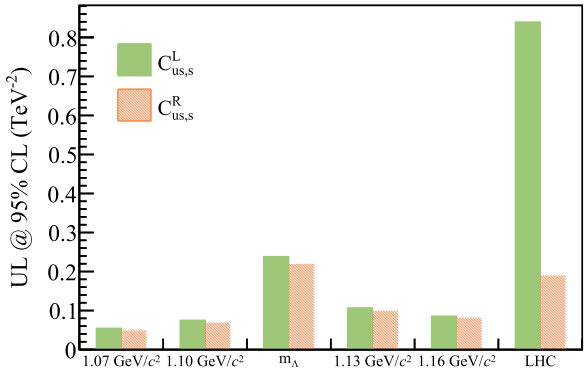

Fig. 4. The 95% C.L. ULs on the Wilson coefficients $C^L_{us,s}$ and $C^R_{us,s}$ derived from the results under different m_χ hypotheses. The constraints derived from the LHC searches [12] are also shown.

icantly improve previous limits derived from the LHC searches for the colored mediators [12] by factors of 15 and 4, respectively.

6. Summary

A search for a dark baryon in the two-body decay $\Xi^- \to \pi^- + \text{invisible}$ is presented using $(10.087 \pm 0.044) \times 10^9$ J/ψ events collected at a CM energy of $\sqrt{s} = 3.097$ GeV with the BESIII detector at the BEPCII collider. No significant signal is observed and the 90% (95%) C.L. ULs on $\mathcal{B}(\Xi^- \to \pi^- + \text{invisible})$ are determined to be 4.2×10^{-5} (5.2×10^{-5}), 6.9×10^{-5} (8.4×10^{-5}), 6.5×10^{-4} (7.6×10^{-4}), 1.1×10^{-4} (1.3×10^{-4}), and 4.5×10^{-5} (5.5×10^{-5}), under the dark baryon mass hypotheses of 1.07 GeV/c^2, 1.10 GeV/c^2, m_Λ, 1.13 GeV/c^2, and 1.16 GeV/c^2, respectively. The constraints obtained on the Wilson coefficients $C^L_{us,s}$ and $C^R_{us,s}$ are more stringent than the previous limits from the LHC searches for the colored mediators.

Data availability

Data will be made available on request.

Declaration of competing interest

The authors declare that they have no known competing financial interests or personal relationships that could have appeared to influence the work reported in this paper.

Acknowledgement

The BESIII Collaboration thanks the staff of BEPCII (https://cstr.cn/31109.02.BEPC) and the IHEP computing center for their strong support. This work is supported in part by National Key R&D Program of China under Contracts Nos. 2023YFA1606000, 2023YFA1606704, 2020YFA0406400; National Natural Science Foundation of China (NSFC) under Contracts Nos. 11635010, 11935015, 11935016, 11935018, 12025502, 12035009, 12035013, 12061131003, 12192260, 12192261, 12192262, 12192263, 12192264, 12192265, 12221005, 12225509, 12235017, 12361141819; the Chinese Academy of Sciences (CAS) Large-Scale Scientific Facility Program; CAS under Contract No. YSBR-101; 100 Talents Program of CAS; The Institute of Nuclear and Particle Physics (INPAC) and Shanghai Key Laboratory for Particle Physics and Cosmology; Agencia Nacional de Investigación y Desarrollo de Chile (ANID), Chile under Contract No. ANID PIA/APOYO AFB230003; German Research Foundation DFG under Contract No. FOR5327; Istituto Nazionale di Fisica Nucleare, Italy; Knut and Alice Wallenberg Foundation under Contracts Nos. Knut and Alice Wallenberg Foundation2021.0174, 2021.0299; Ministry of Development of Turkey under Contract No. DPT2006K-120470; National Research Foundation of Korea under Contract No. National Research Foundation of Korea NRF-2022R1A2C1092335; National Science and Technology fund of Mongolia; Polish National Science Centre under Contract No. 2024/53/B/ST2/00975; Swedish Research Council under Contract No. 2019.04595; U. S. Department of Energy under Contract No. DE-FG02-05ER41374

BESIII Collaboration

M. Ablikim[1], M. N. Achasov[4,94], P. Adlarson[87], X. C. Ai[92], R. Aliberti[41], A. Amoroso[83,84,83,86], Q. An[I,64,80], Y. Bai[63], O. Bakina[42], Y. Ban[52,99], H.-R Bao[72], V. Batozskaya[1,50], K. Begzsuren[38], N. Berger[41], M. Berlowski[50], M. Bertani[29,30], D. Bettoni[33,34], F. Bianchi[83,84,86], E. Bianco[83,84,86], A. Bortone[83,84,86], I. Boyko[42], R. A. Briere[5], A. Brueggemann[77], H. Cai[88], M. H. Cai[44,102,103], X. Cai[1,64], A. Calcaterra[29,30], G. F. Cao[1,72], N. Cao[1,72], S. A. Cetin[68,69], X. Y. Chai[52,99], J. F. Chang[1,64], G. R. Che[49], Y. Z. Che[1,64,72], C. H. Chen[9], Chao Chen[61], G. Chen[1], H. S. Chen[1,72], H. Y. Chen[21], M. L. Chen[1,64,72], S. J. Chen[48], S. L. Chen[51], S. M. Chen[67], T. Chen[1,72], X. R. Chen[37,72], X. T. Chen[1,72], X. Y. Chen[12,98], Y. B. Chen[1,64], Y. Q. Chen[40], Y. Q. Chen[16], Z. Chen[25], Z. J. Chen[26,100], Z. K. Chen[65], S. K. Choi[10], X. Chu[12,98], G. Cibinetto[33,34], F. Cossio[83,86], J. Cottee-Meldrum[71], J. J. Cui[56], H. L. Dai[1,64], J. P. Dai[90], A. Dbeyssi[19], R. E. De Boer[3], D. Dedovich[42], C. Q. Deng[81], Z. Y. Deng[1], A. Denig[41], I. Denysenko[42], M. Destefanis[83,84,86], F. De Mori[83,84,86], B. Ding[1,75], X. X. Ding[52,99], Y. Ding[46], Y. Ding[40], Y. X. Ding[36], J. Dong[1,64], L. Y. Dong[1,72], M. Y. Dong[1,64,72], X. Dong[88], M. C. Du[1], S. X. Du[92], S. X. Du[12,98], Y. Y. Duan[61], P. Egorov[42,93], G. F. Fan[48], J. J. Fan[20], Y. H. Fan[51], J. Fang[1,64], J. Fang[65], S. S. Fang[1,72], W. X. Fang[1], Y. Q. Fang[I,1,64], R. Farinelli[33,34], L. Fava[83,85,86], F. Feldbauer[3], G. Felici[29,30], C. Q. Feng[64,80], J. H. Feng[16], L. Feng[44,102,103], Q. X. Feng[44,102,103], Y. T. Feng[64,80], M. Fritsch[3], C. D. Fu[1], J. L. Fu[72], Y. W. Fu[1,72], H. Gao[72], X. B. Gao[47], Y. Gao[64,80], Y. N. Gao[52,99], Y. N. Gao[20], Y. Y. Gao[36], S. Garbolino[83,86], I. Garzia[33,34,35], P. T. Ge[20], Z. W. Ge[48], C. Geng[65], E. M. Gersabeck[76], A. Gilman[78], K. Goetzen[13], J. D. Gong[40], L. Gong[46], W. X. Gong[1,64], W. Gradl[41], S. Gramigna[33,34,35], M. Greco[83,84,86], M. H. Gu[1,64], Y. T. Gu[15], C. Y. Guan[1,72], A. Q. Guo[37], L. B. Guo[47], M. J. Guo[56], R. P. Guo[55], Y. P. Guo[12,98], A. Guskov[42,93], J. Gutierrez[28], K. L. Han[72], T. T. Han[1], F. Hanisch[3], K. D. Hao[64,80], X. Q. Hao[20], F. A. Harris[74], K. K. He[61], K. L. He[1,72], F. H. Heinsius[3], C. H. Heinz[41], Y. K. Heng[1,64,72], C. Herold[66], P. C. Hong[40], G. Y. Hou[1,72], X. T. Hou[1,72], Y. R. Hou[72], Z. L. Hou[1], H. M. Hu[1,72], J. F. Hu[62,101], Q. P. Hu[64,80], S. L. Hu[12,98], T. Hu[1,64,72], Y. Hu[1], Z. M. Hu[65], G. S. Huang[64,80], K. X. Huang[65], L. Q. Huang[37,72], P. Huang[48], X. T. Huang[56], Y. P. Huang[1], Y. S. Huang[65], T. Hussain[82], N. Hüsken[41], N. In Der Wiesche[77], J. Jackson[28], Q. Ji[1], Q. P. Ji[20], W. Ji[1,72], X. B. Ji[1,72], X. L. Ji[1,64], Y. Y. Ji[56], Z. K. Jia[64,80], D. Jiang[1,72], H. B. Jiang[88], P. C. Jiang[52,99], S. J. Jiang[9], T. J. Jiang[17], X. S. Jiang[1,64,72], Y. Jiang[72], J. B. Jiao[56], J. K. Jiao[40], Z. Jiao[24], S. Jin[48], Y. Jin[75], M. Q. Jing[1,72], X. M. Jing[72], T. Johansson[87], S. Kabana[39], N. Kalantar-Nayestanaki[73], X. L. Kang[9], X. S. Kang[46], M. Kavatsyuk[73], B. C. Ke[92], V. Khachatryan[28], A. Khoukaz[77], R. Kiuchi[1], O. B. Kolcu[68,69], B. Kopf[3], M. Kuessner[3], X. Kui[1,72], N. Kumar[27], A. Kupsc[50,87], W. Kühn[43], Q. Lan[81], W. N. Lan[20], T. T. Lei[64,80], M. Lellmann[41], T. Lenz[41], C. Li[64,80], C. Li[53], C. Li[49], C. H. Li[45], C. K. Li[21], D. M. Li[92], F. Li[1,64], G. Li[1], H. B. Li[1,72], H. J. Li[20], H. N. Li[62,101], Hui Li[49], J. R. Li[67], J. S. Li[65], K. Li[1], K. L. Li[20], K. L. Li[44,102,103], L. J. Li[1,72], Lei Li[54], M. H. Li[49], M. R. Li[1,72], P. L. Li[72], P. R. Li[44,102,103], Q. M. Li[1,72], Q. X. Li[56], R. Li[18,37], S. X. Li[12], T. Li[56], T. Y. Li[49], W. D. Li[1,72], W. G. Li[I,1], X. Li[1,72], X. H. Li[64,80], X. L. Li[56], X. Y. Li[1,8], X. Z. Li[65], Y. Li[20], Y. G. Li[52,99], Y. P. Li[40], Z. J. Li[65], Z. Y. Li[90], H. Liang[64,80], Y. F. Liang[60], Y. T. Liang[37,72], G. R. Liao[14], L. B. Liao[65], M. H. Liao[65], Y. P. Liao[1,72], J. Libby[27], A. Limphirat[66], C. C. Lin[61], D. X. Lin[37,72], L. Q. Lin[45], T. Lin[1], B. J. Liu[1], B. X. Liu[88], C. Liu[40], C. X. Liu[1], F. Liu[1], F. H. Liu[59], Feng Liu[6], G. M. Liu[62,101], H. Liu[44,102,103], H. B. Liu[15], H. H. Liu[1], H. M. Liu[1,72], Huihui Liu[22], J. B. Liu[64,80], J. J. Liu[21], K. Liu[44,102,103], K. Liu[81], K. Y. Liu[46], Ke Liu[23], L. C. Liu[49], Lu Liu[49], M. H. Liu[12,98], P. L. Liu[1], Q. Liu[72], S. B. Liu[64,80], T. Liu[12,98], W. K. Liu[49], W. M. Liu[64,80], W. T. Liu[45], X. Liu[44,102,103], X. Liu[45], X. K. Liu[44,102,103], X. Y. Liu[88], Y. Liu[44,102,103], Y. Liu[92], Yuan Liu[92], Y. B. Liu[49], Z. A. Liu[1,64,72], Z. D. Liu[9], Z. Q. Liu[56], X. C. Lou[1,64,72], F. X. Lu[65], H. J. Lu[24], J. G. Lu[1,64], X. L. Lu[16], Y. Lu[7], Y. H. Lu[1,72], Y. P. Lu[1,64], Z. H. Lu[1,72], C. L. Luo[47], J. R. Luo[65], J. S. Luo[1,72], M. X. Luo[91], T. Luo[12,98], X. L. Luo[1,64], Z. Y. Lyu[23], X. R. Lyu[72,106], Y. F. Lyu[49], Y. H. Lyu[92], F. C. Ma[46], H. L. Ma[1], J. L. Ma[1,72], L. L. Ma[56], L. R. Ma[75], Q. M. Ma[1], R. Q. Ma[1,72], R. Y. Ma[20], T. Ma[64,80], X. T. Ma[1,72], X. Y. Ma[1,64], Y. M. Ma[37], F. E. Maas[19], I. Mackay[78], M. Maggiora[83,84,86], S. Malde[78], Q. A. Malik[82], H. X. Mao[44,102,103], Y. J. Mao[52,99], Z. P. Mao[1], S. Marcello[83,84,86], A. Marshall[71], F. M. Melendi[33,34,35], Y. H. Meng[72], Z. X. Meng[75],

G. Mezzadri[34], H. Miao[1,72], T. J. Min[48], R. E. Mitchell[28], X. H. Mo[1,64,72], B. Moses[28], N. Yu Muchnoi[4,94], J. Muskalla[41], Y. Nefedov[42], F. Nerling[19,96], L. S. Nie[21], I. B. Nikolaev[4,94], Z. Ning[1,64], S. Nisar[11,104], Q. L. Niu[44,102,103], W. D. Niu[12,98], C. Normand[71], S. L. Olsen[10,72], Q. Ouyang[1,64,72], S. Pacetti[29,31,32], X. Pan[61], Y. Pan[63], A. Pathak[10], Y. P. Pei[64,80], M. Pelizaeus[3], H. P. Peng[64,80], X. J. Peng[44,102,103], Y. Y. Peng[44,102,103], K. Peters[13,96], K. Petridis[71], J. L. Ping[47], R. G. Ping[1,72], S. Plura[41], V. Prasad[40], F. Z. Qi[1], H. R. Qi[67], M. Qi[48], S. Qian[1,64], W. B. Qian[72], C. F. Qiao[72], J. H. Qiao[20], J. J. Qin[81], J. L. Qin[61], L. Q. Qin[14], L. Y. Qin[64,80], P. B. Qin[81], X. P. Qin[12,98], X. S. Qin[56], Z. H. Qin[1,64], J. F. Qiu[1], Z. H. Qu[81], J. Rademacker[71], C. F. Redmer[41], A. Rivetti[86], M. Rolo[86], G. Rong[1,72], S. S. Rong[1,72], F. Rosini[29,31,32], Ch Rosner[19], M. Q. Ruan[1,64], N. Salone[50], A. Sarantsev[42,95], Y. Schelhaas[41], K. Schoenning[87], M. Scodeggio[33,34], K. Y. Shan[12,98], W. Shan[25], X. Y. Shan[64,80], Z. J. Shang[44,102,103], J. F. Shangguan[17], L. G. Shao[1,72], M. Shao[64,80], C. P. Shen[12,98], H. F. Shen[1,8], W. H. Shen[72], X. Y. Shen[1,72], B. A. Shi[72], H. Shi[64,80], J. L. Shi[12,98], J. Y. Shi[1], S. Y. Shi[81], X. Shi[1,64], H. L. Song[64,80], J. J. Song[20], T. Z. Song[65], W. M. Song[40], Y. J. Song[12,98], Y. X. Song[52,99,105], S. Sosio[83,84,86], S. Spataro[83,84,86], F. Stieler[41], S. S. Su[46], Y. J. Su[72], G. B. Sun[88], G. X. Sun[1], H. Sun[72], H. K. Sun[1], J. F. Sun[20], K. Sun[67], L. Sun[88], S. S. Sun[1,72], T. Sun[57,97], Y. C. Sun[88], Y. H. Sun[36], Y. J. Sun[64,80], Y. Z. Sun[1], Z. Q. Sun[1,72], Z. T. Sun[56], C. J. Tang[60], G. Y. Tang[1], J. Tang[65], J. J. Tang[64,80], L. F. Tang[45], Y. A. Tang[88], L. Y. Tao[81], M. Tat[78], J. X. Teng[64,80], J. Y. Tian[64,80], W. H. Tian[65], Y. Tian[37], Z. F. Tian[88], I. Uman[68,70], B. Wang[1], B. Wang[65], Bo Wang[64,80], C. Wang[44,102,103], C. Wang[20], Cong Wang[23], D. Y. Wang[52,99], H. J. Wang[44,102,103], J. J. Wang[88], K. Wang[1,64], L. L. Wang[1], L. W. Wang[40], M. Wang[56], M. Wang[64,80], N. Y. Wang[72], S. Wang[12,98], T. Wang[12,98], T. J. Wang[49], W. Wang[65], Wei Wang[81], W. P. Wang[41,64,80,19], X. Wang[52,99], X. F. Wang[44,102,103], X. J. Wang[45], X. L. Wang[12,98], X. N. Wang[1], Y. Wang[67], Y. D. Wang[51], Y. F. Wang[1,8,72], Y. H. Wang[44,102,103], Y. J. Wang[64,80], Y. L. Wang[20], Y. N. Wang[88], Y. Q. Wang[1], Yaqian Wang[18], Yi Wang[67], Yuan Wang[18,37], Z. Wang[1,64], Z. L. Wang[81], Z. L. Wang[2], Z. Q. Wang[12,98], Z. Y. Wang[1,72], D. H. Wei[14], H. R. Wei[49], F. Weidner[77], S. P. Wen[1], Y. R. Wen[45], U. Wiedner[3], G. Wilkinson[78], C. Wu[45], J. F. Wu[1,8], L. H. Wu[1], L. J. Wu[1,72], L. J. Wu[20], Lianjie Wu[20], S. G. Wu[1,72], S. M. Wu[72], X. Wu[12,98], X. H. Wu[40], Y. J. Wu[37], Z. Wu[1,64], L. Xia[64,80], X. M. Xian[45], B. H. Xiang[1,72], D. Xiao[44,102,103], G. Y. Xiao[48], H. Xiao[81], Y. L. Xiao[12,98], Z. J. Xiao[47], C. Xie[48], K. J. Xie[1,72], X. H. Xie[52,99], Y. Xie[56], Y. G. Xie[1,64], Y. H. Xie[6], Z. P. Xie[64,80], T. Y. Xing[1,72], C. J. Xu[65], G. F. Xu[1], H. Y. Xu[2,75], H. Y. Xu[2], M. Xu[64,80], Q. J. Xu[17], Q. N. Xu[36], T. D. Xu[81], W. Xu[1], W. L. Xu[75], X. P. Xu[61], Y. Xu[46], Y. Xu[12,98], Y. C. Xu[89], Z. S. Xu[72], F. Yan[12,98], H. Y. Yan[45], L. Yan[12,98], W. B. Yan[64,80], W. C. Yan[92], W. H. Yan[6], W. P. Yan[20], X. Q. Yan[1,72], H. J. Yang[57,97], H. L. Yang[40], H. X. Yang[1], J. H. Yang[48], R. J. Yang[20], T. Yang[1], Y. Yang[12,98], Y. F. Yang[49], Y. H. Yang[48], Y. Q. Yang[9], Y. X. Yang[1,72], Y. Z. Yang[20], M. Ye[1,64], M. H. Ye[I,8], Z. J. Ye[62,101], Junhao Yin[49], Z. Y. You[65], B. X. Yu[1,64,72], C. X. Yu[49], G. Yu[13], J. S. Yu[26,100], L. Q. Yu[12,98], M. C. Yu[46], T. Yu[81], X. D. Yu[52,99], Y. C. Yu[92], C. Z. Yuan[1,72], H. Yuan[1,72], J. Yuan[40], J. Yuan[51], L. Yuan[2], S. C. Yuan[1,72], X. Q. Yuan[1], Y. Yuan[1,72], Z. Y. Yuan[65], C. X. Yue[45], Ying Yue[20], A. A. Zafar[82], S. H. Zeng[71], X. Zeng[12,98], Y. Zeng[26,100], Yujie Zeng[65], Y. J. Zeng[1,72], X. Y. Zhai[40], Y. H. Zhan[65], A. Q. Zhang[1,72], B. L. Zhang[1,72], B. X. Zhang[1], D. H. Zhang[49], G. Y. Zhang[20], G. Y. Zhang[1,72], H. Zhang[64,80], H. Zhang[92], H. C. Zhang[1,64,72], H. H. Zhang[65], H. Q. Zhang[1,64,72], H. R. Zhang[64,80], H. Y. Zhang[1,64], Jin Zhang[92], J. Zhang[65], J. J. Zhang[58], J. L. Zhang[21], J. Q. Zhang[47], J. S. Zhang[12,98], J. W. Zhang[1,64,72], J. X. Zhang[44,102,103], J. Y. Zhang[1], J. Z. Zhang[1,72], Jianyu Zhang[72], L. M. Zhang[67], Lei Zhang[48], N. Zhang[92], P. Zhang[1,8], Q. Zhang[20], Q. Y. Zhang[40], R. Y. Zhang[44,102,103], S. H. Zhang[1,72], Shulei Zhang[26,100], X. M. Zhang[1], X. Y. Zhang[46], X. Y. Zhang[56], Y. Zhang[1], Y. Zhang[81], Y. T. Zhang[92], Y. H. Zhang[1,64], Y. M. Zhang[45], Y. P. Zhang[64,80], Z. D. Zhang[1], Z. H. Zhang[1], Z. L. Zhang[40], Z. L. Zhang[61], Z. X. Zhang[20], Z. Y. Zhang[88], Z. Y. Zhang[49], Z. Z. Zhang[51], Z. Z. Zhang[20], G. Zhao[1], J. Y. Zhao[1,72], J. Z. Zhao[1,64], L. Zhao[1], L. Zhao[64,80], M. G. Zhao[49], N. Zhao[90], R. P. Zhao[72], S. J. Zhao[92], Y. B. Zhao[1,64], Y. L. Zhao[61], Y. X. Zhao[37,72], Z. G. Zhao[64,80], A. Zhemchugov[42,93], B. Zheng[81], B. M. Zheng[40], J. P. Zheng[1,64], W. J. Zheng[1,72], X. R. Zheng[20], Y. H. Zheng[72,106], B. Zhong[47], C. Zhong[20], H. Zhou[41,56,19], J. Q. Zhou[40], J. Y. Zhou[40], S. Zhou[6], X. Zhou[88], X. K. Zhou[6], X. R. Zhou[64,80], X. Y. Zhou[45], Y. X. Zhou[89], Y. Z. Zhou[12,98], A. N. Zhu[72], J. Zhu[49], K. Zhu[1], K. J. Zhu[1,64,72], K. S. Zhu[12,98], L. Zhu[40], L. X. Zhu[72], S. H. Zhu[79], T. J. Zhu[12,98], W. D. Zhu[47], W. D. Zhu[12,98], W. J. Zhu[1], W. Z. Zhu[20], Y. C. Zhu[64,80], Z. A. Zhu[1,72], X. Y. Zhuang[49], J. H. Zou[1], J. Zu[64,80]

Affiliation Notes

[I] Deceased

Collaboration Institutes

[1] Institute of High Energy Physics, 100049, Beijing, People's Republic of China
[2] Beihang University, 100191, Beijing, People's Republic of China
[3] Bochum Ruhr-University, D-44780, Bochum, Germany
[4] Budker Institute of Nuclear Physics SB RAS (BINP), 630090, Novosibirsk, Russia
[5] Carnegie Mellon University, 15213, Pittsburgh, Pennsylvania, USA
[6] Central China Normal University, 430079, Wuhan, People's Republic of China
[7] Central South University, 410083, Changsha, People's Republic of China
[8] Center of Advanced Science and Technology, 100190, Beijing, People's Republic of China
[9] China University of Geosciences, 430074, Wuhan, People's Republic of China
[10] Chung-Ang University, 06974, Seoul, Republic of Korea
[11] COMSATS University Islamabad, Lahore Campus Defence Road Off Raiwind Road, 54000, Lahore, Pakistan
[12] Fudan University, 200433, Shanghai, People's Republic of China
[13] GSI Helmholtzcentre for Heavy Ion Research GmbH, D-64291, Darmstadt, Germany
[14] Guangxi Normal University, 541004, Guilin, People's Republic of China
[15] Guangxi University, 530004, Nanning, People's Republic of China
[16] Guangxi University of Science and Technology, 545006, Liuzhou, People's Republic of China
[17] Hangzhou Normal University, 310036, Hangzhou, People's Republic of China
[18] Hebei University, 071002, Baoding, People's Republic of China
[19] Helmholtz Institute Mainz, Staudinger Weg 18, D-55099, Mainz, Germany
[20] Henan Normal University, 453007, Xinxiang, People's Republic of China
[21] Henan University, 475004, Kaifeng, People's Republic of China
[22] Henan University of Science and Technology, Luoyang 471003, People's Republic of China
[23] Henan University of Technology, 450001, Zhengzhou, People's Republic of China
[24] Huangshan College, 245000, Huangshan, People's Republic of China
[25] Hunan Normal University, 410081, Changsha, People's Republic of China
[26] Hunan University, 410082, Changsha, People's Republic of China
[27] Indian Institute of Technology Madras, 600036, Chennai, India
[28] Indiana University, 47405, Bloomington, Indiana, USA

[29] INFN Laboratori Nazionali di Frascati
[30] INFN Laboratori Nazionali di Frascati, I-00044, Frascati, Italy
[31] INFN Sezione di Perugia, I-06100, Perugia, Italy
[32] University of Perugia, I-06100, Perugia, Italy
[33] INFN Sezione di Ferrara
[34] INFN Sezione di Ferrara, I-44122, Ferrara, Italy
[35] University of Ferrara, I-44122, Ferrara, Italy
[36] Inner Mongolia University, 010021, Hohhot, People's Republic of China
[37] Institute of Modern Physics, 730000, Lanzhou, People's Republic of China
[38] Institute of Physics and Technology, Mongolian Academy of Sciences, Peace Avenue 54B, 13330, Ulaanbaatar, Mongolia
[39] Instituto de Alta Investigación, Universidad de Tarapacá, Casilla 7D, 1000000, Arica, Chile
[40] Jilin University, 130012, Changchun, People's Republic of China
[41] Johannes Gutenberg University of Mainz, Johann-Joachim-Becher-Weg 45, D-55099, Mainz, Germany
[42] Joint Institute for Nuclear Research, 141980, Dubna Moscow region, Russia
[43] II. Physikalisches Institut, Justus-Liebig-Universitaet Giessen, Heinrich-Buff-Ring 16, D-35392, Giessen, Germany
[44] Lanzhou University, 730000, Lanzhou, People's Republic of China
[45] Liaoning Normal University, 116029, Dalian, People's Republic of China
[46] Liaoning University, 110036, Shenyang, People's Republic of China
[47] Nanjing Normal University, 210023, Nanjing, People's Republic of China
[48] Nanjing University, 210093, Nanjing, People's Republic of China
[49] Nankai University, 300071, Tianjin, People's Republic of China
[50] National Centre for Nuclear Research, 02-093, Warsaw, Poland
[51] North China Electric Power University, 102206, Beijing, People's Republic of China
[52] Peking University, 100871, Beijing, People's Republic of China
[53] Qufu Normal University, 273165, Qufu, People's Republic of China
[54] Renmin University of China, 100872, Beijing, People's Republic of China
[55] Shandong Normal University, 250014, Jinan, People's Republic of China
[56] Shandong University, 250100, Jinan, People's Republic of China
[57] Shanghai Jiao Tong University, 200240, Shanghai, People's Republic of China
[58] Shanxi Normal University, 041004, Linfen, People's Republic of China
[59] Shanxi University, 030006, Taiyuan, People's Republic of China
[60] Sichuan University, 610064, Chengdu, People's Republic of China
[61] Soochow University, 215006, Suzhou, People's Republic of China
[62] South China Normal University, 510006, Guangzhou, People's Republic of China
[63] Southeast University, 211100, Nanjing, People's Republic of China
[64] State Key Laboratory of Particle Detection and Electronics, 100049, Beijing Hefei, People's Republic of China
[65] Sun Yat-Sen University, 510275, Guangzhou, People's Republic of China
[66] Suranaree University of Technology, University Avenue 111, 30000, Nakhon Ratchasima, Thailand
[67] Tsinghua University, 100084, Beijing, People's Republic of China
[68] Turkish Accelerator Center Particle Factory Group
[69] Istinye University, 34010, Istanbul, Türkiye
[70] Near East University, Nicosia Mersin 10, 99138, North Cyprus, Türkiye
[71] H H Wills Physics Laboratory, University of Bristol, Tyndall Avenue, BS8 1TL, Bristol, UK
[72] University of Chinese Academy of Sciences, 100049, Beijing, People's Republic of China
[73] University of Groningen, NL-9747 AA, Groningen, The Netherlands
[74] University of Hawaii, 96822, Honolulu, Hawaii, USA
[75] University of Jinan, 250022, Jinan, People's Republic of China
[76] University of Manchester, Oxford Road, M13 9PL, Manchester, United Kingdom
[77] University of Muenster, Wilhelm-Klemm-Strasse 9, 48149, Muenster, Germany
[78] University of Oxford, Keble Road, OX13RH, Oxford, United Kingdom
[79] University of Science and Technology Liaoning, 114051, Anshan, People's Republic of China
[80] University of Science and Technology of China, 230026, Hefei, People's Republic of China
[81] University of South China, 421001, Hengyang, People's Republic of China
[82] University of the Punjab, Lahore, 54590, Pakistan
[83] University of Turin, INFN
[84] University of Turin, I-10125, Turin, Italy
[85] University of Eastern Piedmont, I-15121, Alessandria, Italy
[86] INFN, I-10125, Turin, Italy
[87] Uppsala University, Box 516, SE-75120, Uppsala, Sweden
[88] Wuhan University, 430072, Wuhan, People's Republic of China
[89] Yantai University, 264005, Yantai, People's Republic of China
[90] Yunnan University, 650500, Kunming, People's Republic of China
[91] Zhejiang University, 310027, Hangzhou, People's Republic of China
[92] Zhengzhou University, 450001, Zhengzhou, People's Republic of China
[93] Moscow Institute of Physics and Technology, 141700, Moscow, Russia
[94] Novosibirsk State University, 630090, Novosibirsk, Russia
[95] NRC Kurchatov Institute, PNPI, 188300, Gatchina, Russia
[96] Goethe University Frankfurt, 60323, Frankfurt am Main, Germany
[97] Key Laboratory for Particle Physics, Astrophysics and Cosmology, Ministry of Education, Institute of Nuclear and Particle Physics, Shanghai Key Laboratory for Particle Physics and Cosmology, 200240, Shanghai, People's Republic of China
[98] Institute of Modern Physics, Key Laboratory of Nuclear Physics and Ion-beam Application (MOE), Fudan University, 200443, Shanghai, People's Republic of China
[99] State Key Laboratory of Nuclear Physics and Technology, Peking University, 100871, Beijing, People's Republic of China
[100] School of Physics and Electronics, Hunan University, 410082, Changsha, China
[101] Guangdong Provincial Key Laboratory of Nuclear Science, Institute of Quantum Matter, South China Normal University, 510006, Guangzhou, China
[102] MOE Frontiers Science Center for Rare Isotopes, Lanzhou University, 730000, Lanzhou, People's Republic of China
[103] Lanzhou Center for Theoretical Physics, Lanzhou University, 730000, Lanzhou, People's Republic of China
[104] Department of Mathematical Sciences, IBA, 75270, Karachi, Pakistan
[105] Ecole Polytechnique Federale de Lausanne (EPFL), CH-1015, Lausanne, Switzerland
[106] Hangzhou Institute for Advanced Study, University of Chinese Academy of Sciences, 310024, Hangzhou, People's Republic of China

References

[1] N. Aghanim et al., Planck Collaboration, Astron. Astrophys. 641 (2020) A6; Erratum: Astron. Astrophys. 652 (2021) C4.
[2] K. Petraki, R.R. Volkas, Int. J. Mod. Phys. A 28 (2013) 01330028.
[3] K.M. Zurek, Phys. Rept. 537 (2014) 91.
[4] B. Fornal, B. Grinstein, Phys. Rev. Lett. 120 (2018) 191801; Erratum: Phys. Rev. Lett. 124 (2020) 219901.
[5] G. Elor, M. Escudero, A. Nelson, Phys. Rev. D 99 (2019) 035031.
[6] A.E. Nelson, H. Xiao, Phys. Rev. D 100 (2019) 075002.
[7] G. Alonso-Álvarez, G. Elor, M. Escudero, Phys. Rev. D 104 (2021) 035028.
[8] J.P. Lees et al. (BABAR Collaboration), Phys. Rev. D 107 (2023) 092001.
[9] J.P. Lees et al. (BABAR Collaboration), Phys. Rev. Lett. 131 (2023) 0201801.
[10] E. Goudzovski, et al., Rep. Prog. Phys. 86 (2023) 016201.
[11] M. Ablikim et al. (BESIII Collaboration), Phys. Rev. D 105 (2022) 071101.
[12] G. Alonso-Álvarez et al., Phys. Rev. D 105 (2022) 115005.
[13] R.M. Baltrusaitis et al. (MARK III Collaboration), Phys. Rev. Lett. 56 (1986) 2140.
[14] M. Ablikim, Chin. Phys. C 46 (2022) 074001.

[15] M. Ablikim et al. (BESIII Collaboration), Nucl. Instrum. Meth. A 614 (2010) 345.
[16] C.H. Yu et al., in: Proceedings of IPAC2016, Busan, Korea, 2016. https://doi.org/10.18429/JACoW-IPAC2016-TUYA01
[17] M. Ablikim et al. (BESIII Collaboration), Chin. Phys. C 44 (2020) 040001.
[18] X. Li et al., Radiat. Detect. Technol. Methods 1 (2017) 13.
[19] Y.X. Guo et al., Radiat. Detect. Technol. Methods 1 (2017) 15.
[20] P. Cao et al., Nucl. Instrum. Meth. A 953 (2020) 163053.
[21] S. Agostinelli et al. (GEANT4 Collaboration), Nucl. Instrum. Meth. A 506 (2003) 250.
[22] K.X. Huang et al., Nucl. Sci. Tech. 33 (2022) 142.
[23] Z.J. Li et al., Front. Phys. 19 (2024) 64201.
[24] Y.T. Liang et al., Nucl. Instrum. Meth. A 603 (2009) 325.
[25] Z.Y. You et al., Chin. Phys. C 32 (2008) 572.
[26] S. Jadach, B.F.L. Ward, Z. Was, Comput. Phys. Commun. 63 (2001) 113009; Comput. Phys. Commun. 130 (2000) 260.
[27] D.J. Lange, Nucl. Instrum. Meth. A 462 (2001) 152. R.G. Ping, Chin. Phys. C 32 (2008) 599.
[28] S. Navas et al. ([Particle Data Group]) Phys. Rev. D 110 (2024) 030001.
[29] J.C. Chen et al., Phys. Rev. D 62 (2000) 034003.
[30] R.L. Yang, R.G. Ping, H. Chen, Chin. Phys. Lett. 31 (2014) 061301.
[31] E. Richter-Was, Phys. Lett. B 303 (1993) 163.
[32] M. Ablikim et al. (BESIII Collaboration), Phys. Rev. D 108 (2023) L031106.
[33] M. Ablikim et al. (BESIII Collaboration), Nature 606 (2022) 64.
[34] M. Ablikim et al. (BESIII Collaboration), Nat. Phys. 15 (2019) 631.
[35] M. Xu et al., Chin. Phys. C 34 (2010) 92.
[36] X.Y. Zhou et al., Comput. Phys. Commun. 258 (2021) 107540.
[37] M. Ablikim et al. (BESIII Collaboration), Phys. Rev. D 93 (2016) 072003.
[38] G. Punzi, eConf C030908 arXiv:physics/038063, 2003.
[39] M. Ablikim et al. (BESIII Collaboration), Phys. Lett. B 852 (2024) 138614.
[40] K.S. Cranmer, Comput. Phys. Commun. 136 (2001) 198.
[41] G. Cowan et al., Eur. Phys. J. C 71 (2011) 1554. Erratum: Eur. Phys. J. C 73 (2013) 2501.